Available online at www.sciencedirect.com
SCIENCE DIRECT®
Journal of Nuclear Materials 353 (2006) 202–208
journal of nuclear materials
www.elsevier.com/locate/jnucmat

A fabrication technique for a UO_2 pellet consisting of UO_2 grains and a continuous W channel on the grain boundary

Jae Ho Yang *, Kun Woo Song, Keon Sik Kim, Youn Ho Jung

Advanced LWR Fuel Development, Korea Atomic Energy Research Institute, Deokjin-dong 150, Yuseong-gu, Daejeon-si 305-600, South Korea

Received 14 November 2005; accepted 11 January 2006

Abstract

A new fabrication process of UO_2–W composite fuel has been studied in order to improve the thermal conductivity of the UO_2 pellet by the addition of a small amount of W. A fabrication process was designed from the phase equilibria among tungsten, tungsten oxides and UO_2. The conventionally sintered UO_2 pellet which contains W particles is heat-treated in an oxidizing gas and then in a reducing gas. In the oxidizing heat-treatment W particles are oxidized and liquid tungsten oxide penetrates within the UO_2 grain boundary, and in the reducing heat-treatment liquid oxide is transformed to solid tungsten which forms a continuous channel along the UO_2 grain boundary. This developed technique can provide a continuous W channel covering UO_2 grains for a UO_2–W composite fuel even with a small amount of a metal phase – below 6 vol.%. The thermal diffusivity of the UO_2–6 vol.%W cermet composite increases by about 80% when compared with that of a pure UO_2 pellet.

1. Introduction

Uranium dioxide is widely used as a fuel material in the nuclear industry, owing to its many advantages. But it has the disadvantage that its thermal conductivity is the lowest of all the kinds of nuclear fuels; metal, carbide, nitride [1]. The thermal conductivity of a nuclear fuel is one of the most important thermo-physical properties that determines the fuel performance in a nuclear reactor. An improvement in the thermal conductivity of the UO_2 pellet leads to a lower fuel temperature, which reduces the fission gas release during a irradiation and it also means a lower stored energy of a nuclear fuel. A lessened stored energy significantly increases the safety margin for the loss of coolant accident (LOCA) [2].

The thermal conductivity of the UO_2 fuel can be greatly enhanced by making a cermet composite which consists of both a continuous body of a highly thermal-conducting metal and UO_2 islands [3–13]. In this cermet, the continuous metal channel can work as a good path for thermal propagation. The conventional cermet fuel should contain a metal phase of at least 30%, usually more than 50%, of the volume of the pellet in order to maintain

* Corresponding author. Tel.: +82 42 868 2813; fax: +82 42 861 7340.
E-mail address: yangjh@kaeri.re.kr (J.H. Yang).

0022-3115/$ - see front matter © 2006 Elsevier B.V. All rights reserved.
doi:10.1016/j.jnucmat.2006.01.019

the metal phase as interconnected. This high volume fraction of a metal requires such a high enrichment of U that the parasitic effect of a metal should be compensated for. Therefore, it is attractive to develop a composite fuel that can contain a metal phase with as small an amount of metal as possible. Hot isostatic pressing (HIP) technique has often offered a method to fabricate a cermet fuel pellet with a small amount of a metal phase [8,14]. However, this technique consists of coating a fuel particle with a metal phase and then pressing the coated particles in a high temperature. It is relatively complicated and time-consuming from the viewpoint of mass production.

In this investigation, a feasibility study was undertaken on how to fabricate a cermet fuel pellet by using only a small amount of metal via simple processes. The candidate metal was tungsten, and the fabrication process was conceptually designed from thermodynamic calculations. We have experimentally found that a small volume of a tungsten phase envelops perfectly the UO_2 grains, forming a continuous channel throughout the pellet, and that it improves the thermal conductivity of the pellet.

2. Experiments

ADU–UO_2 powder was mixed with W powder using a tumbling mixer. The initial weight fraction of the W powder was 9 wt%. The mixed powder was pressed into green pellets and then sintered at 1700 °C for 4 h in hydrogen, and such a sintered UO_2 pellet contains W particles which are dispersed uniformly throughout the pellet. This UO_2 pellet was step-wise annealed under two different annealing conditions. The first step was for oxidizing the W particles; the pellet was annealed at 1400 °C in a CO_2 gas atmosphere for 30 min. In the second step, the annealed pellet was heated to 1650 °C in H_2 and held for 2 h. These annealing temperatures and gas environments were determined by thermodynamic calculations.

The pellets obtained after the first and second step were longitudinally sectioned and polished. Their microstructures were observed with an optical microscope. The grain structure morphology and the cation distribution were measured with both SEM and an electron probe microanalysis. The relative volume ratio of the metal matrix to the UO_2 grain was obtained through an image analyzer program. The phase evolution resulting from the sequential processes – sintering, annealing, and reducing – was characterized by the X-ray diffraction profiles.

Disk samples with a 10-mm diameter and ~1-mm thickness were taken from the W-particle-dispersed UO_2 pellet and a continuous-channel-containing UO_2 pellet for the thermal diffusivity measurements. The thermal diffusivity was measured by the laser flash method [15] from room temperature to 1200 °C in vacuum atmosphere using a laser flash apparatus (Netzsch LFA 427). A uniform heat pulse of a short duration (compared to the transient time through the sample) was incident on the front face of a disc specimen, and the temperature rise on the rear face was recorded. The thermal diffusivities were calculated by using the method developed by Cowan [16], in which the deviations from the idealized behavior caused by the heat losses are corrected. The measured thermal diffusivities were compared with that of the pure UO_2 sample.

The relative difference in the thermal conductivity between the metal and UO_2 phases was measured with a scanning thermal microprobe (CP research) [17,18]. A thermal imaging was achieved by using a resistive thermal element attached to the end of a cantilever which enables an AFM type feedback. The thermal element consists of a bent filament of platinum/10% rhodium. The 'thermal conductivity contrast mode' was used. The amount of power required to maintain the probe at a constant temperature is directly related to the thermal conductivity of the test specimen. The specimens were carefully polished in order to avoid a surface influence on the heat conduction. The thermal data was collected from a 100 μm × 100μm scan area at a scanning speed of 1 Hz.

3. Results and discussion

3.1. Fabrication process design

In order to effectively enhance the thermal conductivity of UO_2 with a small amount of a metal phase, the metal phase should have a high thermal conductivity. A high melting point is also needed from a safety point of view. Tungsten is a good candidate. The fabrication process design is purely based on the thermodynamic relations between UO_2, metal tungsten and the tungsten oxide phases. The free energy changes of the following two oxidation reactions are calculated by using the HSC program [19].

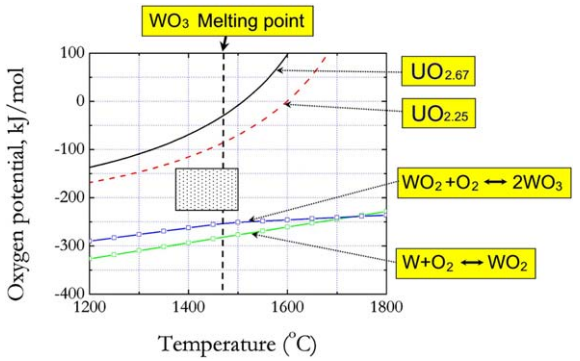

Fig. 1. Equilibrium oxygen potential curves.

$$W + O_2 = WO_2$$

$$WO_2 + \tfrac{1}{2}O_2 = WO_3.$$

Fig. 1 shows the equilibrium free energy of the two oxidation equations above together with the equilibrium oxygen potential curves of the U_3O_8 and U_4O_9 phases [20,21]. The equilibrium oxygen potential of tungsten metal to WO_3 via WO_2 is much lower than that of the U_3O_8 and U_4O_9 phases. This thermodynamic feature makes it possible to selectively oxidize the W to WO_3 in the W-particle-containing UO_2 pellet, with the UO_2 structure being maintained. This WO_3 will be a liquid form if the annealing temperature is higher than the melting point of WO_3 (= about 1470 °C). The oxygen potential range where liquid tungsten oxide and solid cubic UO_2 are stable is denoted as a hatched area in Fig. 1. The liquid tungsten oxide can penetrate between UO_2 grains as in liquid phase sintering and thus a continuous channel of liquid can be formed along the grain boundary in the UO_2 pellet, when the W-dispersed UO_2 pellet is annealed at the conditions of the hatched area in Fig. 1. The liquid tungsten oxide can be reduced to tungsten metal by a heating in hydrogen, thus transforming it to a metallic channel in the UO_2 pellet.

3.2. Fabrication results

Specimens were prepared by following the overall fabrication processes: sintering, annealing, and reducing process. The results are described for each process. Fig. 2(a) and (b) shows the microstructure and the XRD pattern of the sintered UO_2 pellet, respectively. Fig. 2(a) shows that the tungsten particles are uniformly dispersed in the UO_2 pellet. This finding is consistent with the X-ray diffraction

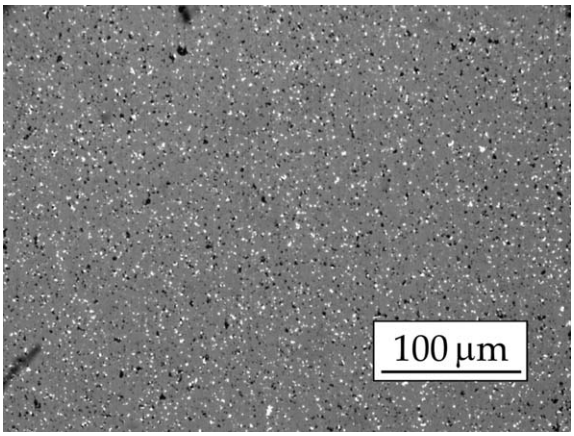

Fig. 2. Optical micrograph (a) and XRD pattern (b) of the as-sintered 9 wt% W dispersed UO_2 pellet. Open circles denote the diffraction lines from tungsten metal.

pattern which reveals a two-phase mixture of UO_2 and metal tungsten [see Fig. 2(b), tungsten is denoted by an open circle].

The above sintered UO_2 pellet was annealed at 1400 °C in a CO_2 atmosphere for 30 min. Thus the tungsten particles in the UO_2 pellet should be oxidized to WO_3 by this annealing process. Fig. 3 shows the SEM image of the annealed UO_2 pellet. The microstructure shows a typical feature of the liquid phase sintered pellet in which a melted phase is continuously precipitated along the grain boundary. The EDS analysis reveals that the grain boundary phase consists of mainly the tungsten oxide and that it additionally contains about 7 at% of uranium cation. It was experimentally found that a liquid phase could be obtained even by an annealing at 1400 °C which is much lower than the melting temperature of WO_3, implying that the dissolution of U in the tungsten oxide phase can lower the melting temperature of the tungsten oxide phase. Fig. 4 shows the X-ray diffraction profile obtained at the

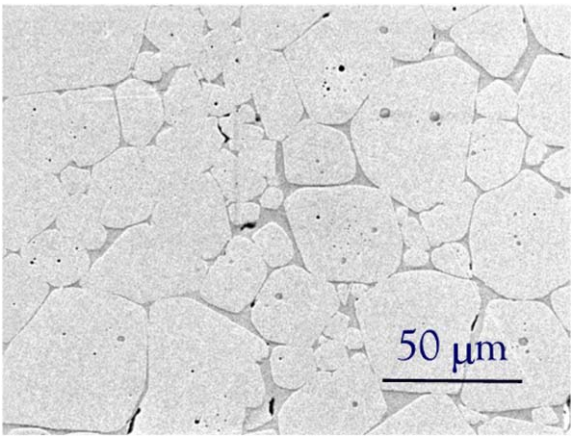

Fig. 3. SEM image of the UO_2–W pellet after the oxidative heat treatment.

surface of the annealed pellet. In addition to the typical UO_2 phase diffraction lines, a new series of diffraction lines, denoted by a filled circle, also appeared in this profile. The diffraction lines of the tungsten metal are not found. The new diffraction lines stem from the grain boundary phase and could be indexed with a unit cell of a cubic symmetry with $a = 3.8064$ Å. From the extinction rule of the $h\,k\,l$ index, the space group of the grain boundary phase is tentatively determined to be Pm3m. The space group and lattice parameter are closely related to the ReO_3 type cubic phase, in which the ReO_6 octahedra form a host lattice by a corner-sharing manner. In this structure, there are cages bonded by the 12 oxygen atoms. It is thought that the tungsten cations are located at the center of the octahedra and the uranium cations are incorporated into the cuboctahedron cages. This structure can be described as an A-cation deficient perovskite, $U_{0.07}WO_3$.

The UO_2–W cermet pellet in which the tungsten metal phase is continuously precipitated along the grain boundary was finally obtained by reducing the annealed pellet. Fig. 5 shows the optical microstructure of the UO_2–W cermet. The UO_2 grains were enveloped in the honeycomb metal frame of tungsten in this fuel. EPMA analysis shows that the grain boundary phase is a pure W. However, about 1 at.% of W was detected in the UO_2 grain, suggesting that there is a small amount of tungsten solubility in the UO_2.

There are several technical issues associated with a homogenous microstructure and an accurate U content in the UO_2–W cermet pellet fabrication process. The first issue is that the densities of W and WO_3 are very different from each other. The oxidation of the W metal particle expanded the pellet volume during the oxidative annealing step. In the reduction step of U_xWO_3 to W+UO_2, the pellet volume should contract due to the volume shrinkage of the tungsten phase. It was found that the voids are often formed in the vicinity where the WO_3 phase had existed before, because the pellet did not completely accommodate the contraction of the tungsten phase in the reduction step. These voids tended to concentrate in the center region of the pellet, producing a pellet that is less dense in the center than on the surface. The second issue is that the vapor pressure of the tungsten oxide phase is relatively high. Some of the tungsten evaporates during the fabrication process. This makes it difficult to precisely control the W content in the UO_2–W composite fuel. These issues were partly solved by controlling the processing parameters such as the annealing temperature, pressure of the

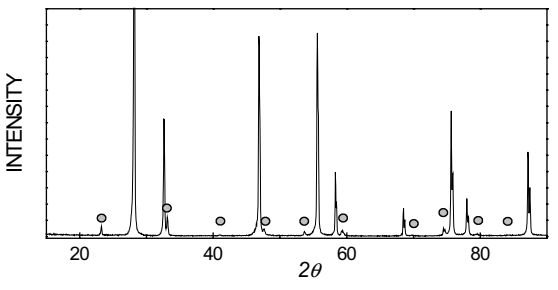

Fig. 4. XRD pattern of the oxidative heat-treated pellet. Filled circles denote the diffraction from the U_xWO_3 type cubic phase.

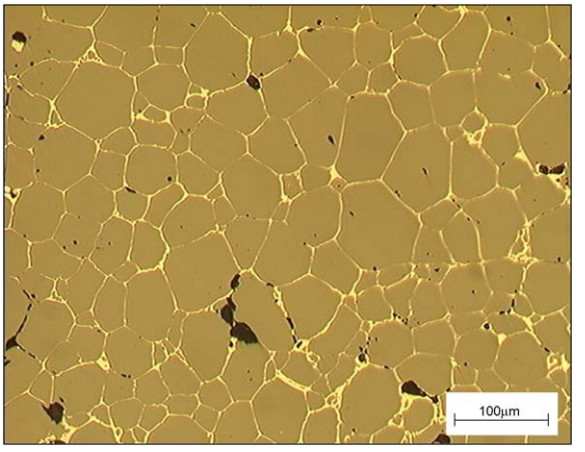

Fig. 5. Optical microscopy image of a continuous W metal channel containing the UO_2 pellet.

annealing atmosphere, microstructure of the tungsten particle dispersed UO_2 pellet, and the pellet size. Especially, a uniformity of the microstructure was achieved when a short composite pellet is fabricated through the developed process.

3.3. Thermophysical properties

The main subject of this study was to increase the thermal conductivity of the UO_2 fuel pellet by using a small amount of the metal phase. The thermal conductivity contour map of the developed pellet surface was obtained on a sub-micrometer scale by scanning thermal microscopy (SThM). Fig. 6(a) and (b) shows a topographical and thermal conductivity contrast image of the polished surface of the pellet sample, respectively. In the topological figure, the grain boundary shape contour could not be detected. However, in the thermal conductivity contrast image, the grain boundary shape was clearly observed. Pores and other defects were also seen in this figure. Fig. 6(c) and (d) shows the profiles of the height and the thermal conductivity along the line indicated in Fig. 6(a) and (b), respectively. It can be observed that the height of the surface does not change considerably along the line. But, the thermal conductivity sharply increases at the grain boundary. This fact clearly indicates that the highly thermal conductive phase is continuously formed along the grain boundary and the thermal conductivity of this pellet is increased by this grain boundary phase.

Disk samples with a 10 mm diameter and ~1 mm thickness were taken from the tungsten-channel-containing UO_2–W composite for the thermal diffusivity measurements. By using an image analyzer program [22] and optical micrographs, the relative volume fraction of the metal tungsten was determined to be 6 vol.% from the average area fraction of the tungsten for both sides of the sample. In order to compare the channeling effect of the tungsten metal phase on the thermal diffusivity enhancement, a 6 vol.% W dispered–UO_2 pellet was prepared through the conventional sintering process. The thermal diffusivities of the UO_2, the 6 vol.% W dispersed–UO_2, and the tungsten-channel-containing UO_2–W composite pellets were measured and compared.

Fig. 7 shows the ratios of the thermal diffusivity of the tungsten-channel-containing UO_2–W composite to pure UO_2 together with that of W–dispersed–UO_2 to pure UO_2 at various temperatures. In the case of the developed tungsten-channel-containing UO_2–W composite, the thermal diffusivity is 50–80% greater than the typical UO_2 fuel [23,24]. Particularly, the thermal diffusivity was enhanced more in the high temperature range. This is because the thermal diffusivity of the ceramic UO_2 decreased more rapidly than the metal tungsten as the temperature increased. In the 6 vol.% W–dispersed–UO_2 pellet, the thermal diffusivity is also increased. However, the increment is much smaller than that of the tungsten-channel-containing UO_2–W composite having the same amount of W phase.

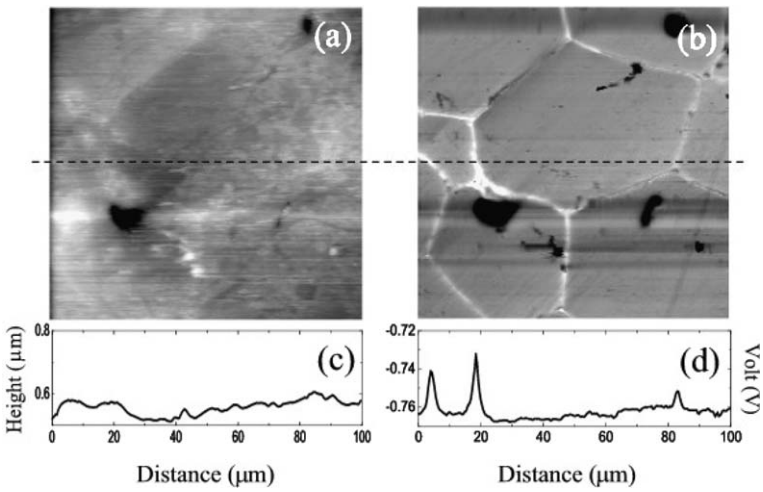

Fig. 6. Topographical and scanning thermal microscope image of the W channel containing UO_2 pellet. (a) Topographical image. (b) SThM image (c) surface height variation across the line indicated in (a), and (d) thermal conductivity distribution across the line indicated in (b).

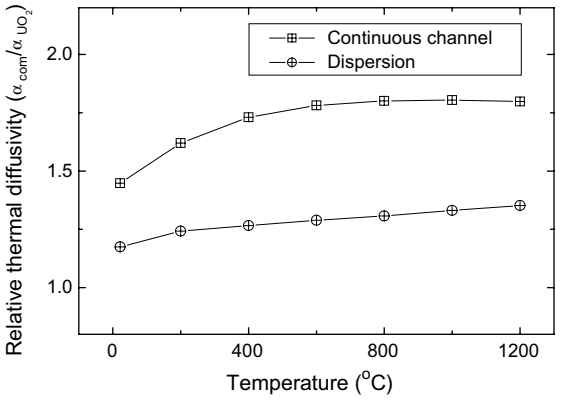

Fig. 7. Relative thermal diffusivities of the tungsten channel containing and tungsten particle dispersed UO_2 pellets to pure UO_2.

Particulate composites such as ceramic-particle-reinforced metal matrix composites have been extensively investigated since they are used in many applications from structural materials to electric devices. Understanding the effects of the microstructural characteristics of inclusions on the thermal properties of composite materials has been a topic of considerable theoretical interest [25–30]. Maxwell [25] derived the equation of an effective thermal conductivity of a spherical particulate dispersed composite. He considered the idealized case of a perfect interface contact between the particle and the matrix. Hasselman and Johnson [26] extended the classical work of Maxwell to consider the interface effect and particle size and derived a Maxwell–Garnett type effective medium approximation (EMA) for calculating the effective thermal conductivity.

According to their calculations, the effective thermal conductivity of a composite can be enhanced further when an higher thermal conductive phase forms a matrix (continuous channel) rather than an inclusion. In an ideal case, the effective thermal conductivity of the 6 vol.% of the tungsten-channel-containing UO_2 composite is calculated to be about 50–100% greater than that of the 6 vol.% W dispersed UO_2 pellet. In our experimental results, the thermal diffusivity of the continuous W–metal-containing UO_2 composite is about 30–40% greater than that of the simply W–particle-dispersed UO_2. The thermal conductivity is a product of the heat capacity, density and thermal diffusivity. When we ignore the heat capacity and density dependence on the microstructure, the thermal diffusivity difference can represent the thermal conductivity difference. Then, the measured diffusivity enhancement of the W channel containing UO_2 is somewhat smaller than the calculated value. The discrepancy could be due to the imperfect interface between W and UO_2, the density of the composite and the W containment in the UO_2 grain, etc. Nevertheless, a continuous metal channel more effectively enhances the thermal conductivity of the composite than the dispersion type.

4. Conclusion

Based on the theory of the phase equilibria among tungsten, tungsten oxides, and UO_2, we have developed a novel fabrication process in which a continuous tungsten-channel-containing UO_2 pellet can be produced from a tungsten-particle-dispersed UO_2 pellet through specific annealing and reducing steps. In the annealing step in an oxidizing gas, tungsten particles are oxidized and then become liquid tungsten oxide, which, in turn, penetrates between the UO_2 grains to form a continuous liquid channel. In the reducing step in hydrogen, the liquid oxide is reduced and then transformed to a solid tungsten channel. This technique creates a metal-channel-containing ceramic composite even with a small amount of the metal phase of about 6 vol.%, in contrast to the conventional cermet fuel which requires about 50 vol.% of metal to make a continuous metal channel.

The thermal diffusivity above 600 °C of the UO_2–6 vol.%W cermet was larger by about 80% and 40% than those of the pure UO_2 and W particle-dispersed UO_2 pellet, respectively. These results for the thermal diffusivity of the UO_2–6 vol.%W cermet confirm that the enhancement in the thermal diffusivity is due to the continuous tungsten channel.

Acknowledgement

This study has been carried out under the Nuclear R&D Program by MOST (Ministry of Science and Technology) in Korea.

References

[1] J.D.B. Lambert, R. Strain, in: Oxide fuels, Nuclear Materials Part 1, Materials Science and Technology, VCH publishers, 1994, p. 109.
[2] M. Gavrilas, P. Hejzlar, N.E. Todreas, Y. Shatilla, in: Safety Features of Operating Light Water Reactors of Western Design, CRC press, 1995, p. 105.
[3] J. Porta, C. Ailland, S. Baldi, J. Nucl. Mat. 274 (1999) 174.

[4] V. Troyanov, V. Popov, Iu. Baranaev, Progr. Nucl. Energy 38 (2001) 267.
[5] G. Ondracek, B. Kanellakopulos, J. Nucl. Mater. 29 (1969) 169.
[6] B. Francois, J.P. Stora, J. Nucl. Mater. 130 (1985) 473.
[7] D.A. Howl, J. Nucl. Mater. 33 (1969) 138.
[8] P. Weimar, F. Thummler, H. Bumm, J. Nucl. Mater. 31 (1969) 215.
[9] T.J. Downar, S.M.M. Deavitt, S.T. Revankar, A.A. Solomon, T.K. Kim, ICONE10-22305, 2002.
[10] A. Fernandez, R.J.M. Konings, J. Somers, J. Nucl. Mater. 319 (2003) 44.
[11] M.V. Krishnaiah, G. Seenivasan, P. Srirama Murti, C.K. Mathews, J. Alloy Comp. 353 (2003) 315.
[12] K. Bakker, F.C. Klaassen, R.P.C. Schram, A. Hogenbirk, R.K. Meulekamp, A. Bos, H. Rakhorst, C.A. Mol, Nuc. Technol. 146 (2004) 325.
[13] M.A. Pouchon, M. Nakamura, Ch. Hellwig, F. Ingold, C. Degueldre, J. Nucl. Mater. 319 (2003) 37.
[14] L. Schwartz, C.M. Lukaniuk, T.H. Etsell, Adv. Eng. Mater. 1 (1999) 111.
[15] W.J. Parker, R.J. Jenkins, C.P. Butter, G.L. Abbot, J. Appl. Phys. 32 (1961) 1679.
[16] R.D. Cowan, J. Appl. Phys. 34 (1963) 1679.
[17] A. Majumdar, Annu. Rev. Mater. Sci. 29 (1999) 505.
[18] S. Gomes, N. Trannoy, P. Grossel, Meas. Sci. Technol. 10 (1999) 805.
[19] A. Roine, Outokumpu HSC Chemistry for Windows, Ver. 2.0, Outokumpu Research Oy, Pori, Finland, 1995.
[20] C. Guéneau, M. Baichi, D. Labroche, C. Chatillon, B. Sundman, J. Nucl. Mater. 304 (2002) 161.
[21] D. Labroche, O. Dugne, C. Chatillon, J. Nucl. Mater. 312 (2003) 21.
[22] Image Pro Plus, Media Cybernetics, 2002, U.S.A.
[23] H.J. Lee, C.W. Kim, J. Kor. Nucl. Soc. 8 (1976) 81.
[24] J.K. Fink, J. Nucl. Mater. 279 (2000) 1.
[25] J.C. Maxwell, vol. 1, Pergamon, Oxford, 1904.
[26] D.P.H. Hasselman, L.F. Johnson, J. Comp. Mater. 21 (1987) 508.
[27] C-W. Nan, R. Birringer, D.R. Clarke, H. Gleiter, J. Appl. Phys. 81 (1997) 6692.
[28] D.M. Staicu, D. Jeulin, M. Beauvy, M. Laurent, High Temp. High Pressures 33 (2001) 293.
[29] A. Decarlis, M. Jaeger, Scripta Mater. 44 (2001) 1955.
[30] T.C. Lim, Mater. Lett. 54 (2002) 152.